Remote Sensing Letters, 2014
Vol. 5, No. 9, 803–812, http://dx.doi.org/10.1080/2150704X.2014.967882

Measuring fire spread rates from repeat pass airborne thermal infrared imagery

Douglas A. Stow[a]*, Philip J. Riggan[b], Emanual J. Storey[a], and Lloyd L. Coulter[a]

[a]*Department of Geography, San Diego State University, San Diego, CA, USA;* [b]*Pacific Southwest Research Station, United States Forest Service, Riverside, CA, USA*

(*Received 29 July 2014; accepted 16 September 2014*)

The objective is to evaluate procedures for direct measurement of fire spread rates (FSRs) based on archived repeat pass airborne thermal infrared (ATIR) imagery and to identify requirements for more refined measurements of FSR and environmental factors that influence FSR. Flaming front positions are delineated on sequential FireMapper ATIR images captured at relatively short repeat intervals enabling fire spread vectors and units to also be delineated. This approach provides the only means for estimating FSR for wildfires at spatial scales in the order of 10^1–10^3 m and timescales from 10^2 to 10^5 s. Magnitudes of estimated FSR from the time sequential ATIR approach for the 2002 Williams fire in southern California tested here are reasonable, given the fire conditions are within the range of rates reported in the literature for wildland fires in Mediterranean shrublands.

1. Introduction

The western US has experienced an extraordinary number of large, destructive wildfires over the past 15 years. Adaptation of fire management and response practices to such fires will require better understanding of fire behaviour, more timely fire intelligence data and more sophisticated fuel and fire behaviour models to evaluate expected fire behaviour in support of tactical fire suppression and decisions regarding strategic management of fuels.

From the standpoints of fire science, wildfire management and particularly emergency response and community evacuation, the primary fire behaviour property of interest is fire spread rate (FSR), which is also referred to as rate of spread. Unfortunately, ground-level measurements of FSR for actual wildfires at landscape-level spatial scales and timescales in the order of few minutes to an hour have been intractable (Alexander and Cruz 2013). Most direct measurements of FSR found in the literature are derived from laboratory observations (table-top or wind tunnel experiment) (Finney et al. 2010; Marino et al. 2012) or from observations of prescribed fires for small field plots in wildland areas. Instrumentation can be employed in advance of control burns to support direct (e.g., ground-based thermocouples) or visual observations for study plots ranging between 10 × 10 m and 750 × 750 m (Bilgili and Saglam 2003; Cruz et al. 2013; Van Wilgen, Le Maitre, and Kruger 1985). However, this is not possible for wildland fires, which tend to burn in more extreme weather conditions than do prescribed fires. Time-averaged FSR of wildland fires can be derived over extensive areas by measuring distances between fire perimeters, which are delineated from anecdotal information from firefighters, aerial spotter flights or remotely sensed imagery (Riggan and Tissell 2009). However, with

*Corresponding author. Email: stow@mail.sdsu.edu

inconsistent data quality or infrequently captured remote sensing data, it is difficult to determine accurately the displacement distance between flaming front locations. Thus, it is difficult to study FSRs and direction and associate them with driving factors (e.g., weather, topography or vegetation fuel properties) with much certainty or detail.

Remote sensing provides a means for observing and measuring FSR, pre-fire vegetation distributions and quantifying aspects of FSR that are attributable to spatial fuel, terrain and wind variability. Airborne thermal infrared (ATIR) imaging systems based on frame array sensors provide the potential to directly observe actual wildland fire spread processes (not just prescribed fires) and measure FSR at spatial scales in the order of 10^1–10^3 m and timescales from 10^2 to 10^5 s. ATIR systems have not been explicitly employed to estimate FSR at relatively short timescales because their primary mission has been monitoring the extent (perimeter) of wildland or prescribed fires in support of fire suppression and emergency evacuation activities. FSR has been estimated when supporting fire perimeter mapping objectives; however, the imaging flight pattern strategy (relatively infrequent repeat interval) and orientation (along the spreading axes of fires) for fire perimeter mapping are limited in determining FSR at short timescales and over large spatial extents. There is little published literature on the use of time sequential remote sensing imagery for measuring FSR over relatively short time intervals, one example being measurements with an extended dynamic range imaging spectrometer of a prescribed fire in the Brazilian Cerrado (Riggan, Tissell, and Lockwood 2010). Ononye, Vodacek, and Saber (2007) provide useful insights into the delineation of active fire front locations from airborne multispectral imagery. The objective of this paper is to evaluate procedures for direct measurement of FSR based on the extant repeat pass ATIR data and to identify requirements for more refined measurements of FSR and environmental factors that influence FSR.

2. Data

The United States Department of Agriculture Forest Service (USFS) and Pacific Southwest Research Station (PSW) developed an airborne remote sensing system for high-resolution, quantitative fire measurements and mapping at short-, mid- and long-wave infrared wavelengths (Riggan et al. 2004; Riggan and Hoffman 2003*).* The system incorporates a high-dynamic-range indium gallium arsenide camera and FireMapper 2.0 imaging radiometers, in order to measure the very high radiances of wildland fires and are the only instruments widely applied today in fire research and management. The FireMapper system has primarily been utilized to map perimeters, to measure radiant fire intensity and energy flux and to determine the effectiveness of fire suppression actions, including aerial fire-retardant application for wildfires in the western US and Brazil (Riggan et al. 2004; Riggan and Tissell 2009). FireMapper images of wildland fires have been transmitted by satellite communications, orthorectified, assembled into georeferenced mosaics and displayed at http://www.fireimaging.com/ to provide incident command teams and the public with a current, detailed and synoptic view of fire spread and activity.

The PSW FireMapper fire imaging system was deployed aboard a USFS research aircraft in late September 2002 during a wildland fire event within the San Dimas Experimental Forest that was known as the Williams fire and primarily burned as a crown fire through chaparral vegetation. FireMapper data were mostly acquired from a series of parallel, partially overlapping passes, providing multitemporal coverage of the Williams fire at nominal spatial resolutions ranging between 5 and 9 m. At that time, FireMapper did not incorporate an inertial motion unit (IMU) for tracking sensor attitude, and instead a low precision global navigation satellite system (GNSS) was utilized. FireMapper image data used for this study were acquired on 23 September 2002, between 14:00 and 15:15 local time (Pacific Daylight Time) in a series of seven passes. Nearly, all of the active fire areas were imaged twice and three times during the imaging mission.

Wind speed and direction from the San Dimas Remote Automated Weather Station (RAWS) data archive were acquired for the Tanbark Flats station, matching the date and time of the FireMapper image data utilized in this study. A digital elevation model (DEM) based on a 10-m raster was obtained from the United States Geologic Survey (http://earthexplorer.usgs.gov). ArcGIS 10.3 Spatial Analyst tools were used to calculate topographic slope and aspect based on the DEM.

3. Methods

Archived FireMapper images that had been captured with a relatively short repeat pass interval (compared to typical missions where the emphasis is mapping an entire fire perimeter) were selected for the study. Images were geometrically processed to achieve implicit spatial registration. Active flaming fronts of registered images were manually delineated, as were fire spread vectors and associated landscape segments. Median and maximum FSR were estimated for each fire spread sequence and a frequency distribution of FSR estimates was derived. Relationships between FSR estimates and wind speed and direction, terrain and fuel conditions data were evaluated.

Image geoprocessing is a critical procedure for reliably estimating FSR from repeat pass ATIR images, with the most important requirement being precise image-to-image registration (Stow 1999). In this case, the images were captured in an ad hoc rather than using a repeat station imaging approach (Stow, Coulter, and Baer 2003; Coulter, Stow, and Baer 2003), such that they were captured from different sensor station positions with different view geometries. This meant that image registration could only be achieved implicitly by attempting to orthorectify each image precisely so that they shared a common coordinate system and spatial resolution with minimal relief displacement and sensor distortion.

The lack of IMU and precise GNSS data meant that a traditional, labour-intensive approach to orthorectification was required. Horizontal and vertical ground reference data were obtained and utilized as part of the orthorectification process. National Agriculture Imaging Program (NAIP) colour imagery with 1-m spatial resolution was obtained from the United States Geological Survey and utilized for collecting horizontal ground control data. Gridded light detection and ranging (LIDAR) data collected for the US Forest Service on 16–17 July 2007 that represented bare ground elevations were used for collecting vertical control. Ground control points were matched between the FireMapper and NAIP images by an analyst, and elevations at these locations were obtained from the LIDAR digital terrain model. Tie points were collected between overlapping FireMapper image frames for each flight line, and a unique triangulation solution was obtained for each flight line. Following triangulation, individual orthorectified-FireMapper image frames were output and mosaicked using the most nadir-viewing portions of each image frame. Locating corresponding ground control points within the FireMapper and NAIP imagery was complicated by the spectral and spatial resolution differences between the images, as well as the fact that ground features were often obscured by fire flames and/or smouldering ash.

After orthorectifying each image as well as possible, further corrections were applied to sub-frames containing active fire zones by extracting them and shifting the origins of their map models (corner coordinates) in the horizontal (*x* and *y*) directions. This was performed iteratively until locational differences between non-moving (smouldering) hotspots of burned areas in the image sets were minimized to the sub-pixel level.

Sequences of two or three orthorectified and registered images of the much overlapping image extents containing segments of the active fire front were compiled for analysis of FSRs. Definable flaming front locations on each image of a sequence were delineated manually through visual interpretation in reference to cell values at or just exceeding a benchmark value of 100°C – used to define the highest temperature of non-fire areas (Beyers et al. 2007). The flaming front boundary is manifest as the gradient between zones of distinctly high temperature (expressing fire activity) and low temperature background values (consistent with unburned surfaces). Although active flaming fronts were more clearly distinguishable from unburned areas than were post-burn zones of intermediate temperature (smouldering materials or less intense flames), the spatial resolutions of the images are such that some convolving of flame and non-flame portions of the fire front occurs. For this reason, active flaming front locations were delineated conservatively, by constructing boundaries at the edges or partially within high-temperature cells whose values suggest temperature mixing. This cartographic smoothing or generalization is also appropriate because delineating pixel edges strictly would render unrealistic geometric shapes. We refer to the polygon formed by the sequential flaming front curves and the lateral sides that connect the end points at which they are no longer clearly definable as a fire spread unit. The topographic characteristics and fuel conditions within this fire spread unit (along with wind speed and direction) control the FSR estimated by the displacement of the flaming fronts.

Vectors of fire front displacement between sequential stages of the fire were manually constructed as line features between (and generally normal to) the flaming fronts described earlier. Inferences of fire spread direction were based on visual interpretation, by considering the temperature profiles and geometric relationships of the flaming fronts. We used the logical rule that fire movement along a curvilinear advancing front occurs between shortest path distances. To reduce the margin of potential error in comparing fire front displacement from imperfectly aligned images, displacements of less than 3 pixels in length (24–30 m) were omitted. Because there is some variability in direction (and even more in distance) within fire spread units, spread vectors were delineated at regular 10- or 20-m intervals along primary fire fronts (depending on the length of fire fronts) in order to ensure consistent measurements of each vector and delineations for each unit. Attributes of length and direction were determined for each displacement vector. FSR was determined by the displacement distance per unit time between sequential TIR images. Median and maximum spread rates were determined from at least 10 displacement vectors for each fire spread unit.

A frequency distribution of FSR estimates for 73 definable fire spread units was obtained. FSR estimates were compared with hourly mean wind speed and direction data from the Tanbark CA RAWS station, which is located approximately 250 m from the northeast flank of the Williams fire at the time of imaging.

4. Results

Active fire fronts and spread vectors associated with a sample fire spread unit, based on the FireMapper images of the Williams fire and delineation techniques described earlier, are depicted in Figures 1 and 2. Fire fronts are portrayed as curvilinear segments based on the sharp temperature gradient between the unburned and active fire areas. Spread vectors

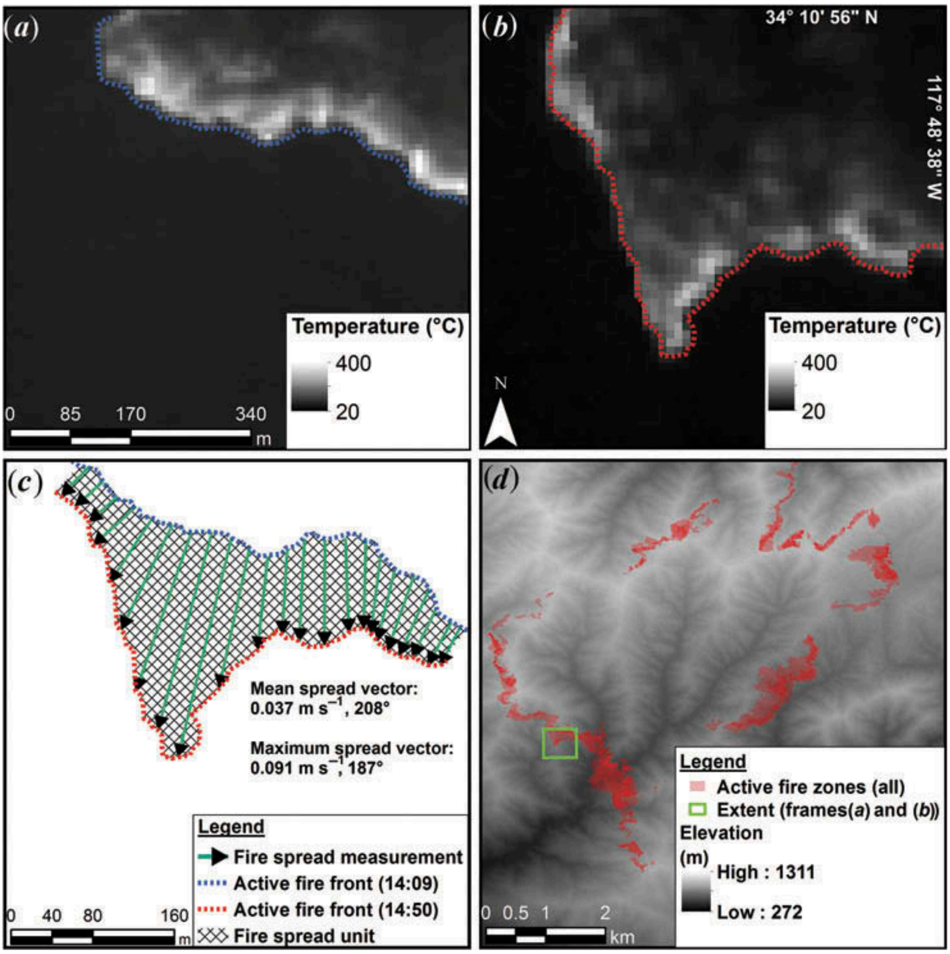

Figure 1. Two-time-period sequence illustrating FSR measurements for a portion of the Williams fire perimeter. (*a*) and (*b*) Co-registered FireMapper thermal infrared images covering the same extent, captured 41 minutes apart. (*c*) Map of delineated fire front locations, fire spread unit and fire spread vectors, with mean and maximum spread vector rate and direction provided. (*d*) Location of fire spread unit (green rectangle) within the overall active burning portion of the Williams Fire in relation to surface elevation; all active fire zones that had been mapped are shown in red.

along the lateral flanks of the fire spread unit are more subjectively delineated, but represent a conservative estimate of the advancing fire front positions in the sequence. Fire spread units with tri-temporal image coverage provide enhanced assessment of fire behaviour, thereby allowing for interpretations of shifting fire directions relative to wind or topographic factors (Figure 2). Shorter intervals between passes and a higher degree of image registration precision would have been necessary to reliably capture the fire spread dynamics of this and several other portions of the Williams fire.

Histograms of mean and maximum FSR values for 73 fire front segments (612 fire spread vectors) derived from the perimeter of the Williams fire within a 1.25-hour period are shown in Figure 3. Mean FSRs (Figure 3(*a*)) range from 0.01 to 0.3 ms^{-1}, with the right-skewed histogram distribution. Over half of the segments have FSRs of less than

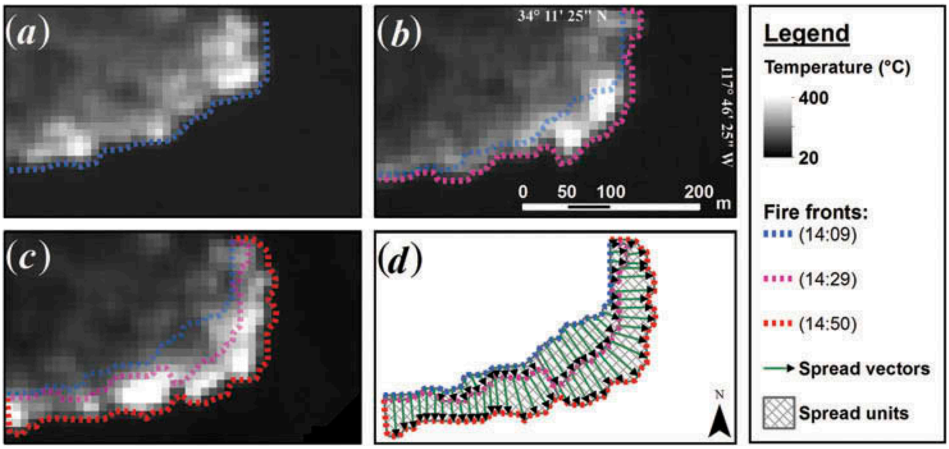

Figure 2. Three-time-period sequence illustrating FSR measurements for a portion of the Williams Fire perimeter. (*a*), (*b*) and (*c*) Co-registered FireMapper thermal infrared images covering the same extent, captured 20 and 21 minutes apart, and (*d*) map of delineated fire front locations (three time periods), fire spread unit and fire spread vectors. The shorter time interval between passes facilitated more certain determination of fire spread vectors than was the case for the fire spread feature depicted in Figure 1.

0.03 ms^{-1}. Maximum FSRs (Figure 3(*b*)) range from 0.01 to 0.5 $ms^{-1}$and exhibit a right-skewed distribution. Only 4 of the 60 segments exhibit spread rates < 0.2 ms^{-1}.

A scatterplot of mean and maximum spread rates against mean and maximum direction, respectively, is shown in Figure 4. The fastest rates are associated with fire spread towards the southwest, west and northwest, on the western and north-western flanks of the fire perimeter. The fastest spread vector has a rate of 0.5 ms^{-1} in the direction 205° (S/SW). The predominant wind direction at the Tanbark Flats RAWS was north-westerly from 14:00 to 15:00 and shifted to a predominant south-easterly direction during the second hour. Median wind speed was 3.1 ms^{-1} during the first hour and 2.2 ms^{-1} during the 15:00 hour. This suggests that the fastest spreading fire fronts were driven by mild Santa Ana-like (dry, north–north-easterly) wind conditions, which was the predominant weather pattern during this stage of the Williams fire.

5. Discussion and conclusions

Magnitudes of estimated FSR from the time sequential ATIR imaging approach tested for the fire conditions of the Williams fire are in line with prior estimates from ground-based observations. According to Alexander and Cruz (2013), FSR for crown fires in shrublands range from 0.01 to 1 ms^{-1}. Fire spread vector directions derived from the procedures are consistent with the general wind flow implied by the limited available wind data and in relation to their locations along the fire perimeter (i.e., advancing and backing fire front locations). These FSR measurements for the Williams fire are based on data from a suboptimal image collection strategy for estimating FSRs and could benefit from higher-frequency image capture to better track more detailed fire spread patterns.

In addition to a well-designed image acquisition plan, another key to making accurate, fine-scale measurements of displaced fire objects (and therefore FSR) is precise

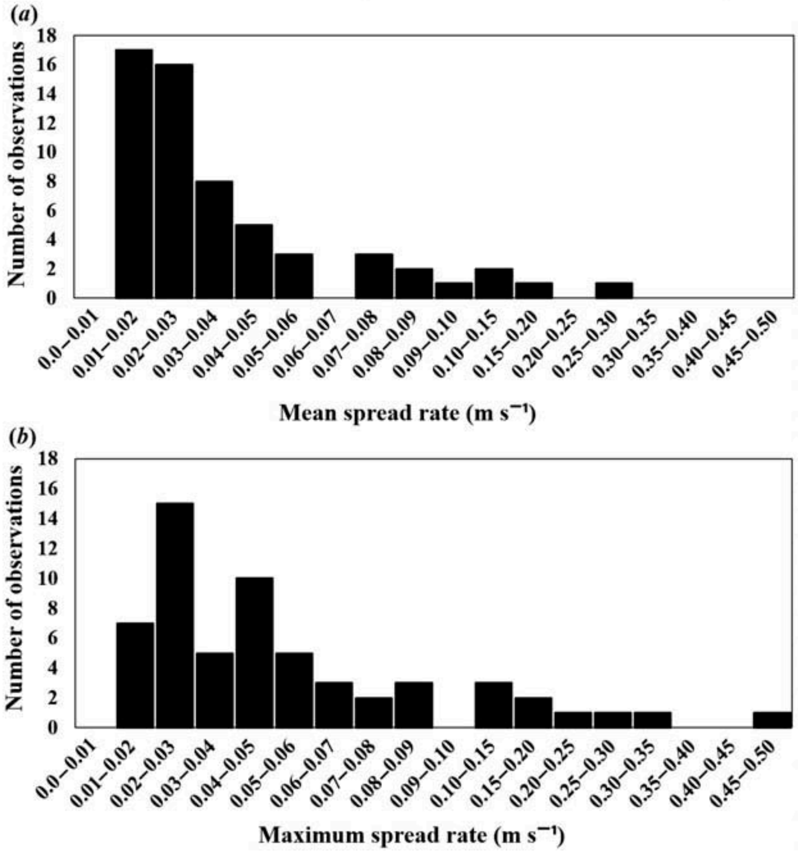

Figure 3. Histograms of (*a*) mean and (*b*) maximum FSR values for 73 fire front segments (612 fire spread vectors) derived from the perimeter of the Williams fire within a 1.25-hour period. FSR intervals are 0.01 from 0 to 0.10 ms^{-1} and 0.05 ms^{-1} for > 0.10 ms^{-1}.

registration or co-alignment of time sequential images. A repeat station image (RSI) acquisition and registration approach that has been demonstrated to achieve registration with errors less than one or two pixels, even for airborne images finer than 8-cm spatial resolution (Coulter, Stow, and Baer 2003; Stow, Coulter, and Baer 2003; Coulter and Stow 2005, 2008; Coulter et al. 2012), will help to ensure precise registration and can be applied in conjunction with a true orthorectification approach to geometric processing. The novel RSI approach utilizes location-based triggering to repeat image observations over time and replicate view geometries. When RSI images are co-registered on a frame-by-frame basis (preserving matched view geometry) using simple image transformations, explicit and precise image registration is obtained.

While the ability to make reliable measurements of landscape-level FSRs is potentially transformative in terms of studying landscape controls on fire behaviour, validating and verifying fire spread model simulation results, and for fire management purposes, determining the validity of such measurements is challenging because of the inability to obtain suitable ground reference data during wildland fire events. Determining the validity and reliability of FSR measurements from this retrospective study is essentially impossible.

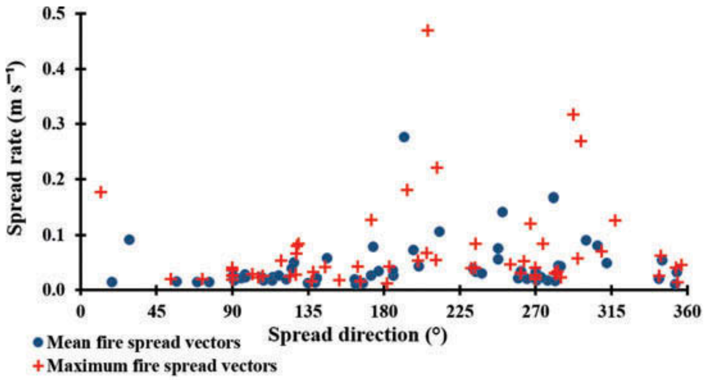

Figure 4. Scatterplot of mean (blue dot) and maximum (red plus) spread rates against mean (blue dot) and maximum mean (red plus) fire spread direction, respectively. North = 0° (and also 360°).

We envision and plan to test in subsequent studies an analytical approach to directly relate remote sensing measurements of fire properties to wind, topographic and pre-fire vegetation reflectance properties and patterns. A visualization example of a fire spread unit (with associated spread vectors) overlaid on vegetation life form map that is draped over a three-dimensional terrain model plot is shown in Figure 5. Direct measurements of FSR will provide data for validating model simulated fire processes in operational and state-of-the-art research models being adapted for operational tools of the future. With proper design and adaptive control of imaging specifications, ATIR imaging systems provide the potential to directly observe actual wildland fire spread processes (not just prescribed fires) and measure FSR at spatial and temporal scales that enable landscape-level studies of factors that control the spread of wildland fire.

Figure 5. Visualization of a fire spread unit (with associated spread vectors) overlaid on vegetation life form map that is draped over a three-dimensional terrain model plot. The figure demonstrates the potential for visually analysing FSR relationships with terrain (slope and aspect) and vegetation-type distributions. Quantitative relationships can also be assessed at the level of the fire spread unit.

Funding

Funding for this study was provided by an American Recovery and Reinvestment Award (ARRA) through the US Forest Service (JV-11279702-101) – SDSU Grant G00008499, Philip Riggan and Douglas Stow, Principal Investigators.

References

Alexander, M., and M. Cruz. 2013. "Assessing the Effect of Foliar Moisture on the Spread Rate of Crown Fires." *International Journal of Wildland Fire* 22: 415–427. doi:10.1071/WF12008.

Beyers, J., P. Riggan, D. Weise, T. Paysen, and M. Narog. 2007. *Age-Class Mosaics and Wind-Driven Fire: Further Fuel for the Debate*. USFS Project Number 07-1-2-10. Boise, ID: Joint Fire Science Program.

Bilgili, E., and B. Saglam. 2003. "Fire Behavior in Maquis Fuels in Turkey." *Forest Ecology and Management* 184: 201–207. doi:10.1016/S0378-1127(03)00208-1.

Coulter, L., and D. Stow. 2005. "Detailed Change Detection Using High Spatial Resolution Frame Center Matched Aerial Photography." Proceedings of the 20th Biennial Workshop on Aerial Photography, Videography, and High Resolution Digital Imagery for Resource Assessment, Weslaco, TX, October 4–6.

Coulter, L., and D. Stow. 2008. "Assessment of the Spatial Co-Registration of Multitemporal Imagery from Large Format Digital Cameras in the Context of Detailed Change Detection." *Sensors* 8: 2161–2173. doi:10.3390/s8042161.

Coulter, L., D. Stow, and S. Baer. 2003. "A Frame Center Matching Technique for Precise Registration of Multitemporal Airborne Frame Imagery." *IEEE Transactions on Geoscience and Remote Sensing* 41 (11): 2436–2444. doi:10.1109/TGRS.2003.819191.

Coulter, L., D. Stow, Y. H. Tsai, C. Chavis, C. Lippitt, G. Fraley, and R. McCreight. 2012. "Automated Detection of People and Vehicles in Natural Environments Using High Temporal Resolution Airborne Remote Sensing." Proceedings of the ASPRS 2012 annual conference, Sacramento, CA, March 19–23.

Cruz, M. G., W. L. McCaw, W. R. Anderson, and J. S. Gould. 2013. "Fire Behaviour Modelling in Semi-Arid Mallee-Heath Shrublands of Southern Australia." *Environmental Modelling & Software* 40: 21–34. doi:10.1016/j.envsoft.2012.07.003.

Finney, M. A., J. D. Cohen, I. C. Grenfell, and K. M. Yedinak. 2010. "An Examination of Fire Spread Thresholds in Discontinuous Fuel Beds." *International Journal of Wildland Fire* 19: 163–170. doi:10.1071/WF07177.

Marino, E., J.-L. Dupuy, F. Pimont, M. Guijarro, C. Hernando, and R. Linn. 2012. "Fuel Bulk Density and Fuel Moisture Content Effects on Fire Rate of Spread: A Comparison between FIRETEC Model Predictions and Experimental Results in Shrub Fuels." *Journal of Fire Sciences* 30: 277–299. doi:10.1177/0734904111434286.

Ononye, A. E., A. Vodacek, and E. Saber. 2007. "Automated Extraction of Fire Line Parameters from Multispectral Infrared Images." *Remote Sensing of Environment* 108 (2): 179–188. doi:10.1016/j.rse.2006.09.029.

Riggan, P. J., and J. W. Hoffman. 2003. "Firemapper™: A Thermal-Imaging Radiometer for Wildfire Research and Operations." Proceedings of the IEEE Aerospace Conference, Paper No. 1522, Big Sky, March 8–15. IEEE.

Riggan, P. J., R. G. Tissel, R. N. Lockwood, J. A. Brass, J. Pereira, S. Miranda, A. C. Miranda, T. Campos, and R. Higgins. 2004. "Remote Measurement of Energy and Carbon Flux from Wildfires in Brazil." *Ecological Applications* 14: 855–872. doi:10.1890/02-5162.

Riggan, P. J., and R. G. Tissell. 2009. "Airborne Remote Sensing of Wildland Fires." In *Wildland Fires and Air Pollution, Developments in Environmental Sciences*, Vol. 8, edited by A. Bytnerowicz, M. Arbaugh, A. Riebau, and C. Andersen, 139–168. Amsterdam: Elsevier.

Riggan, P. J., R. G. Tissell, and R. N. Lockwood. 2010. "Remote measurement of the 1992 Tapera prescribed fire at the Reserva Ecològica do IBGE." In *Efeitos do regime de fogo sobre a estrutura de comunidades de Cerrado: Projeto Fogo*, edited by H. S. Miranda, 144. Brasília: Instituto Brasileiro do Meio Ambiente e dos Recursos Naturais Renováveis.

Stow, D. 1999. "Reducing the Effects of Misregistration on Pixel-Level Change Detection." *Remote Sensing Letters – International Journal of Remote Sensing* 20: 2477–2483. doi:10.1080/014311699212137.

Stow, D., L. Coulter, and S. Baer. 2003. “A Frame Centre Matching Approach to Registration for Change Detection with Fine Spatial Resolution Multi-Temporal Imagery.” *International Journal of Remote Sensing* 24: 3873–3879. doi:10.1080/0143116031000152309.

Van Wilgen, B., D. Le Maitre, and F. Kruger. 1985. “Fire Behaviour in South African Fynbos (Macchia) Vegetation and Predictions from Rothermel’s Fire Model.” *The Journal of Applied Ecology* 22: 207–216. doi:10.2307/2403338.

Remote Sensing Letters, 2014
Vol. 5, No. 11, 1001, http://dx.doi.org/10.1080/2150704X.2014.987576

Corrigendum

Stow, D.A., Riggan, P.J., Storey, E.J., and Coulter, L.L. (2014). **Measuring fire spread rates from repeat pass airborne thermal infrared imagery.** *Remote Sensing Letters*, 5(7–9), pp. 803–812. http://dx.doi.org/10.1080/2150704X.2014.967882.

When the above article was first published online and in print, the initial 'J.' was erroneously included in the third author's name. It should read Emanual A. Storey.